第37卷第5期
2018年10月

红外与毫米波学报
J. Infrared Millim. Waves

Vol. 37, No. 5
October, 2018

文章编号: 1001-9014(2018)05-0523-05

DOI: 10.11972/j.issn.1001-9014.2018.05.003

Ultrafast terahertz modulation characteristics of organolead halide perovskite films revealed by time-resolved terahertz spectroscopy

ZHANG Bo[1*], LYU Long-Feng[2], SHEN Jing-Ling[1*]

(1. Key Laboratory of Terahertz Optoelectronics, Ministry of Education, Beijing Advanced Innovation Center for Imaging Technology, Beijing Key Laboratory for Terahertz Spectroscopy and Imaging, Beijing Key Laboratory of Metamaterials and Devices, Department of Physics, Capital Normal University, Beijing 100048, China;
2. Key Laboratory of Luminescence and Optical Information, Ministry of Education, Institute of Optoelectronic Technology, Beijing Jiaotong University, Beijing 100044, China)

Abstract: Ultrafast terahertz (THz) modulation characteristics of organolead halide perovskite films ($CH_3NH_3PbI_3$ and $CH_3NH_3PbI_{3-x}Cl_x$) were investigated on picosecond time scales using time-resolved THz spectroscopy. Upon photo-excitation, a transient decrease in THz transmission was observed. Compared with $CH_3NH_3PbI_3$, $CH_3NH_3PbI_{3-x}Cl_x$ showed a better modulation depth (10%) within the range of the photo-excitation powers used. The mechanism underpinning this photoconductive ultrafast response was determined by measuring the transmission properties and calculating the carrier density. The larger crystalline bulk of the $CH_3NH_3PbI_{3-x}Cl_x$ film produced higher carrier densities than the $CH_3NH_3PbI_3$ film. These results demonstrate that $CH_3NH_3PbI_{3-x}Cl_x$ films are promising materials for developing high-performance THz modulators and ultrafast switchable THz photoelectric devices.

Key words: Terahertz, organolead halide perovskite, ultrafast modulation
PACS: 02.50.Ng, 42.65.Re

太赫兹时间分辨系统研究有机卤化物钙钛矿薄膜的超快太赫兹调制

张 波[1*], 吕龙锋[2], 沈京玲[1*]

(1. 首都师范大学 物理系 北京市太赫兹波谱与成像重点实验室 太赫兹光电子学教育部重点实验室 北京成像技术高精尖创新中心,北京 100048;
2. 北京交通大学 光电子研究所 发光与光信息技术教育部重点实验室,北京 100044)

摘要: 研究了利用太赫兹时间分辨系统研究有机卤化物钙钛矿薄膜($CH_3NH_3PbI_3$ and $CH_3NH_3PbI_{3-x}Cl_x$)的皮秒尺度的超快太赫兹调制特性. 在光激发作用下出现了太赫兹透射波的瞬时下降. 相比于 $CH_3NH_3PbI_3$ 薄膜, 在光激发作用下 $CH_3NH_3PbI_{3-x}Cl_x$ 薄膜展现了更高的调制深度(10%). 通过测算材料的电导率及载流子浓度,其调制机理为瞬态光激发载流子浓度上升. 实验结果表明,$CH_3NH_3PbI_{3-x}Cl_x$ 薄膜可作为一种高效超快太赫兹调制器件.

关 键 词: 太赫兹; 有机卤化物钙钛矿; 超快调制

中图分类号: 0433.4 **文献标识码:** *A*

Introduction

Organometal halide perovskites have attracted considerable attention because of their excellent photoelectric properties, such as their high absorption coefficients, balanced long-range electron/hole transport lengths, low recombination rate, and tunable bandgap. Tremendous efforts have been made to investigate halide perovskite-based materials for applications in solar cells, light emit-

Received date: 2018-01-11, **revised date:** 2018-04-27 **收稿日期:** 2018-01-11, **修回日期:** 2018-04-27
Foundation items: Supported by the National Natural Science Foundation of China (61505125)
Biography: ZHANG Bo (1984-), male, Beijing, associate professor, research area focus on terahertz modulation.
* **Corresponding author:** E-mail: bzhang@cnu.edu.cn, sjl-phy@cnu.edu.cn

ting diodes, lasers, and other optoelectronic devices [1-5]. Compared with the traditional dye-sensitized solar cells, the overall power conversion efficiency of organometal halide perovskite-based solar cells has rapidly increased, up to 20.1% [6]. Some investigations of these materials are based on directly probing the charge carrier dynamics, such as the carrier lifetime, mobility, and diffusion length, by using time-resolved photoluminescence and optical pump-terahertz probes [7-13]. Determining the dynamics of the photo-excited carriers in $CH_3NH_3PbI_3$ films should provide a deeper understanding of the mechanisms that give rise to the high performance of hybrid perovskite-based devices.

Recently, a broadband optically controlled terahertz (THz) device was successfully produced by increasing the charge carrier density at the $CH_3NH_3PbI_3$/Si interface [14]. The efficiency obtained in devices using the mixed halide perovskite material $CH_3NH_3PbI_{3-x}Cl_x$ as both an absorber and electron transporter was higher than when using a $CH_3NH_3PbI_3$ film [5]; it is thus important to study $CH_3NH_3PbI_{3-x}Cl_x$ films with regard to their ultrafast THz modulation characteristics.

In this study, the ultrafast THz modulation characteristics of organolead halide perovskite films ($CH_3NH_3PbI_3$ and $CH_3NH_3PbI_{3-x}Cl_x$) were investigated on picosecond time scales using time-resolved THz spectroscopy. Under photo-excitation, a transient decrease in the THz transmission could be observed. The mechanism underpinning this photoconductive ultrafast response was then determined by measuring the transmission properties and calculating the carrier density.

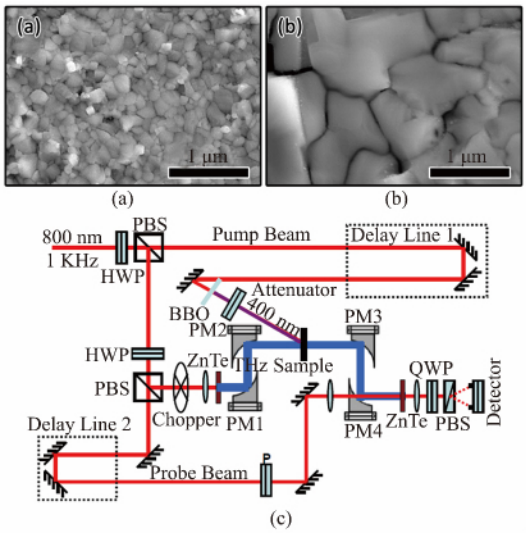

Fig. 1 Scanning electron microscope (SEM) images of (a) $CH_3NH_3PbI_3$ and (b) $CH_3NH_3PbI_{3-x}Cl_x$ films. (c) Experimental setup for the femtosecond optical pump-THz probe measurements

图1 (a) $CH_3NH_3PbI_3$ 薄膜扫描电镜图,(b) $CH_3NH_3PbI_{3-x}Cl_x$ 薄膜扫描电镜图,(c) 飞秒光泵浦太赫兹探测装置图

1 Experiments

In our experiment, $CH_3NH_3PbI_3$ and $CH_3NH_3PbI_{3-x}Cl_x$ thin films were deposited directly onto quartz substrates via solution processing. The $CH_3NH_3PbI_3$ sample was prepared by a solvent-induced one-step deposition. A perovskite solution (45 wt%) was prepared by dissolving CH_3NH_3I and PbI_2 in dimethylformamide, which was then spin-coated on a quartz substrate. During the spin-coating process, 800 ? L of chlorobenzene was quickly dropped onto the substrate. The resulting film (about 300 nm thick) was dried at 100 °C for 15 min. A scanning electron microscopy (SEM) image of the $CH_3NH_3PbI_3$ film is shown in Fig. 1 (a). The $CH_3NH_3PbI_{3-x}Cl_x$ film was fabricated by N_2-assisted one-step deposition. The perovskite solution consisting of CH_3NH_3I and $PbCl_2$ in dimethylformamide was spin-coated on a quartz substrate. Subsequently, the film was treated with a high pressure N_2 flow for about 10 s. The film (about 300 nm thick) was then dried at 100℃ for 150 min; an SEM image of the $CH_3NH_3PbI_{3-x}Cl_x$ film is shown in Fig. 1(b).

An optical pump-THz probe spectroscopy system was used to measure the ultrafast responses of all the samples, as shown in Fig. 1(c). The time-resolved THz spectroscope was driven by a Ti: sapphire amplifier system with a 1 kHz repetition rate and a central wavelength of 800 nm. The THz pulse, generated by <110> oriented ZnTe crystals, was normally incident on the films. The optical path of the pump and THz beams was controlled by two electronically movable stages. The pulses were frequency-doubled to 400 nm in a β-BaB_2O_4 crystal. The pump intensity (240 $\mu J/cm^2$) was used with an adjustable attenuator. By adjusting the optical path between the THz beam and the pump beam, ultrafast responses with various time delays could be measured for the samples excited by the pump pulse.

2 Results and discussions

Figure 2(a) shows the normalized power spectra for THz transmission through the $CH_3NH_3PbI_3$ film under various levels of laser irradiance. In general, the THz transmission power decreased gradually as the laser intensity was increased, dropping to 92% of the original value at an intensity of 240 $\mu J/cm^2$. Figure 2(b) shows the normalized power spectra for THz transmission through the $CH_3NH_3PbI_{3-x}Cl_x$ film under various levels of laser irradiance. Compared with the $CH_3NH_3PbI_3$ film, the THz transmission power decreased to 90% of the original value at the same intensity (240 $\mu J/cm^2$).

Figure 3(a) shows the dependence of the amplitude transmission, averaged over a frequency window ranging from 0.2 to 2.6 THz, as a function of the modulation beam's power. At these photo-excitation intensities, the transmission power through the $CH_3NH_3PbI_{3-x}Cl_x$ film is lower than for the $CH_3NH_3PbI_3$ film. To evaluate the modulation performance of the films, the modulation depth (MD), defined as the change in the integrated

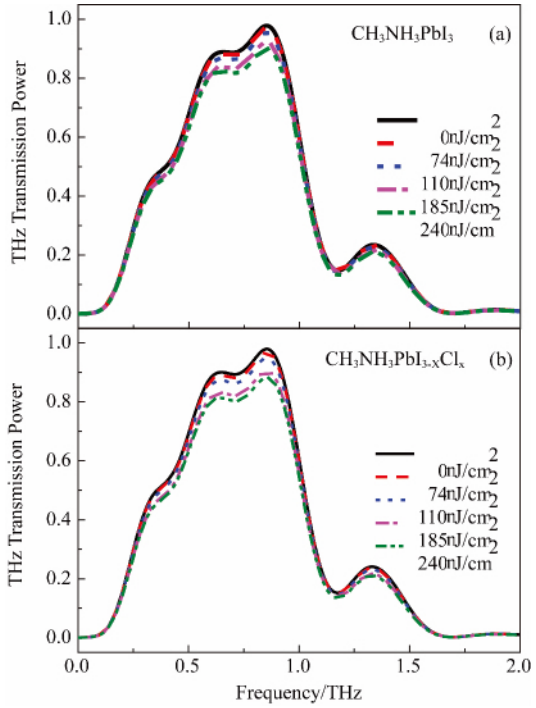

Fig. 2　Measured THz waveforms transmitted through (a) the $CH_3NH_3PbI_3$ film and (b) the $CH_3NH_3PbI_{3-x}Cl_x$ film under different photo-excitation powers

图 2　不同光激发强度下(a) $CH_3NH_3PbI_3$ 薄膜太赫兹波透射谱及(b) $CH_3NH_3PbI_{3-x}Cl_x$ 薄膜太赫兹波透射谱

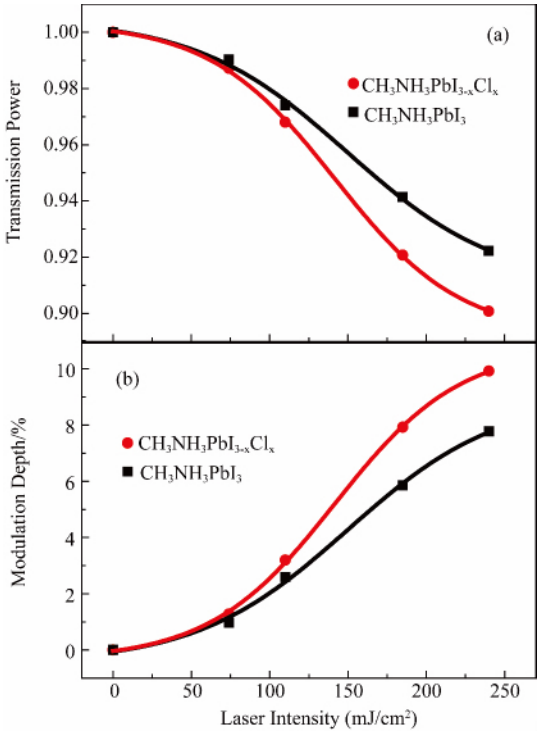

Fig. 3　(a) THz power transmission and (b) modulation factor for $CH_3NH_3PbI_3$ and $CH_3NH_3PbI_{3-x}Cl_x$ films, averaged over a frequency window in the 0.2 ~ 2.6 THz range as a function of the laser intensity

图 3　0.2 ~ 2.6 THz 太赫兹波谱范围内 $CH_3NH_3PbI_3$ 薄膜及 $CH_3NH_3PbI_{3-x}Cl_x$ 薄膜的太赫兹透射强度及调制因子与激发光强的关系

transmitted THz power caused by the photo-excitation intensity, is:

$$MD = \frac{\int P_{laser\text{-}off}(\omega)\,d\omega - \int P_{laser\text{-}on}\omega(d\omega)}{\int P_{laser\text{-}off}(\omega)\,d\omega} \quad ,(1)$$

where $P_{laser\text{-}on}(\omega)$ and $P_{laser\text{-}off}(\omega)$ is the transmitted THz power when the laser is switched on and off, respectively [15-19]. The THz transmission MDs at various optical excitation levels are shown in Fig. 3(b). The MD of the $CH_3NH_3PbI_{3-x}Cl_x$ film is 10% at a pump intensity of 240 $\mu J/cm^2$. However, the MD of the $CH_3NH_3PbI_3$ film is 8% under the same conditions. Generally, the $CH_3NH_3PbI_{3-x}Cl_x$ film has more advantageous properties because it can be used as an active all-optical device for THz waves over a wide frequency range (0.2 ~ 2.6 THz).

The response of the organometal halide perovskite films under external optical excitation was investigated using an optically pumped THz probe system. The power of the pumping beam was modulated with an attenuator. The THz pulse had a delay with respect to the pump beam to ensure that the pulse excited the film. The transmitted THz signal decreased when the pump beam intensity reached 240 $\mu J/cm^2$. The normalized optical pump-terahertz probe results for the two films reveal differences in the THz photoconductivity decay dynamics (Fig. 4). Sharp decreases in the THz peak values for the

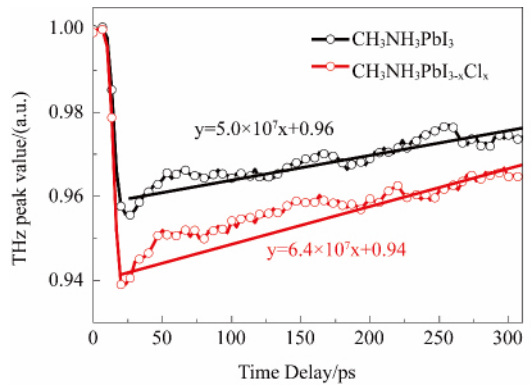

Fig. 4　Changes in the THz waveform maxima with photo-excitations for different time delays

图 4　光泵浦时间延时与太赫兹峰值的变化关系

$CH_3NH_3PbI_3$ and $CH_3NH_3PbI_{3-x}Cl_x$ films are observed and the carrier recombination time response shows almost a 1 ns rise time for both films, as calculated via a linear fit (Fig. 4). However, the $CH_3NH_3PbI_{3-x}Cl_x$ film demonstrates a better modulation depth for the THz peak value compared with the $CH_3NH_3PbI_3$ film.

To investigate the modulation mechanism in the terahertz photoconductivity decay dynamics, the frequency-

dependent equivalent complex conductivity $\sigma(\omega)$ of the films can be determined from the measured transmission spectra with:

$$\frac{E(\omega)}{E_0(\omega)} = \frac{n_s + 1}{n_s + 1 + dZ_0\sigma(\omega)} \quad ,(2)$$

where $n_s = 1.96$ is the refractive index of the quartz substrate, $Z_0 = 377\ \Omega$ is the impedance of free space, ω is the angular frequency of the incident light, and $d = 300$ nm is the film thickness [20-21]. The real ($\sigma_r(\omega)$) and imaginary ($\sigma_i(\omega)$) parts of the calculated photoconductivity in the $CH_3NH_3PbI_3$ film and the $CH_3NH_3PbI_{3-x}Cl_x$ film at different time delays are shown in Figs. 5(a-d). Many studies indicate that the Drude-Smith model could provide a superior fit to both the real and imaginary parts of the conductivity for many materials [22-23]. The Drude-Smith model is expressed as:

$$\tilde{\sigma}(\omega) = \frac{Ne^2\tau/m^*}{1 - i\omega\tau}\left[1 + \frac{c}{1 - i\omega\tau}\right] \quad , \quad (3)$$

where c is a measure of velocity persistence and its negative value implies a predominance of backscattering, N is the carrier density, e is the elementary charge, m^* is the electron effective mass, and τ is the characteristic scattering time. The carrier density of the $CH_3NH_3PbI_3$ film increased to $N = 5.28 \times 10^{17}/cm^3$ with an optical excitation of 240 $\mu J/cm^2$, causing the largest change in the modulation depth (8%). However, the carrier density of the $CH_3NH_3PbI_{3-x}Cl_x$ film increased to $N = 7.04 \times 10^{17}/cm^3$ with the same optical excitation; this resulted in a modulation depth change of 10%, as shown in Fig. 5(e). The larger crystalline bulk of the $CH_3NH_3PbI_{3-x}Cl_x$ film produces higher carrier densities compared with the $CH_3NH_3PbI_3$ film. After photo-excitation, the carrier density returned to a value close to the original. With a 300 ps time delay, the carrier density of the $CH_3NH_3PbI_3$ film decreased to $N = 3.23 \times 10^{17}/cm^3$ and the modulation depth decreased by 4.4%. When the carrier density of the $CH_3NH_3PbI_{3-x}Cl_x$ film decreased to $N = 4.83 \times 10^{17}/cm^3$, the modulation depth decreased by 5.8%. This decrease in carrier density led to a fall in the optical conductivity, and thus the THz transmission returned to the initial state.

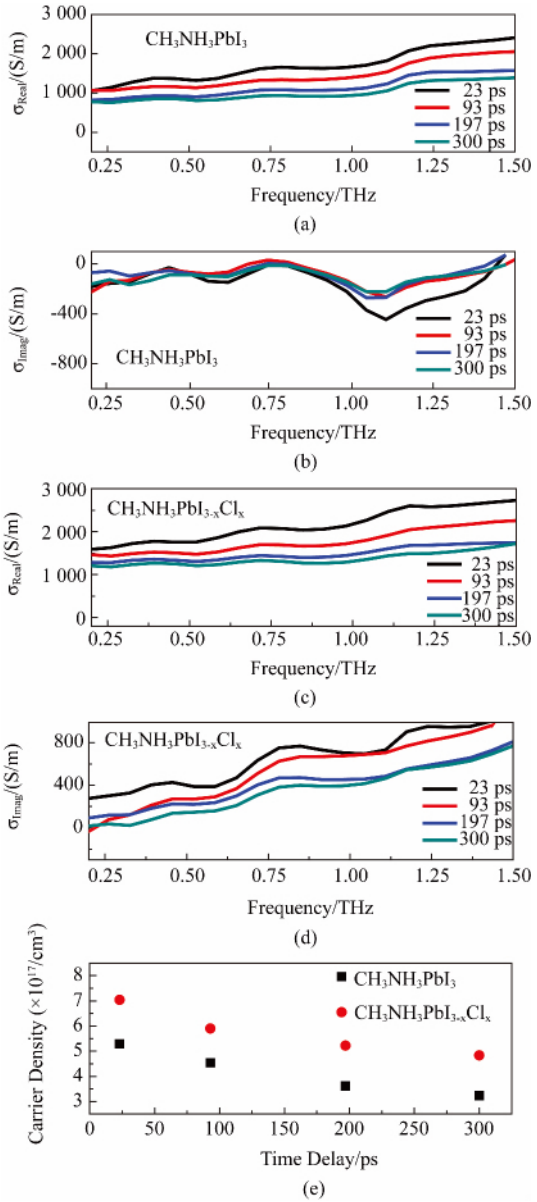

Fig. 5 Effective conductivities (a-d) and carrier densities (e) of the two films after various time delays at 240 $\mu J/cm^2$ light irradiance. The calculated $CH_3NH_3PbI_3$ film as (a) real and (b) imaginary and $CH_3NH_3PbI_{3-x}Cl_x$ film (c) real and (d) imaginary photoconductivities

图5 240 $\mu J/cm^2$ 光激发下不同延时的有效电导率(a-d)及载流子浓度(e). $CH_3NH_3PbI_3$ 薄膜的电导率实部(a)及虚部(b),$CH_3NH_3PbI_{3-x}Cl_x$ 薄膜的电导率的实部(c)及虚部(d)

3 Conclusions

In summary, we used a direct, noncontact method to investigate the influence of the optical pump power on the photo-generated carrier relaxation process. A transient decrease in the THz transmission on a picosecond timescale was observed under light excitation. The $CH_3NH_3PbI_{3-x}Cl_x$ film showed a better modulation depth within the same range of photo-excitation intensities than the $CH_3NH_3PbI_3$ film. The results show the intrinsic photophysics of semiconducting organometal halide perovskites, which have applications in high-performance THz modulators and ultrafast switchable THz photoelectric devices. These materials may also make terahertz filtering and other such applications possible in the future.

Acknowledgements

We acknowledge Prof. Xinke Wang for his helpful measurement and discussions.

References

[1] Burschka J, Pellet N, Moon N, *et al*. Sequential deposition as a route to high-performance perovskite-sensitized solar cells, *Nature*, 2013, **499**: 316-319.

(下转第532页)

Journal of Selected Topics in Quantum Electronics, 2014, **20**(6): 354-363.

[5] Perenzoni M, Perenzoni D, Stoppa D. A 64×64-pixels digital silicon photomultiplier direct TOF sensor with 100 M photons/s/pixel background rejection and imaging/altimeter mode with 0.14% precision up to 6 km for spacecraft navigation and landing [J]. *IEEE Journal of Solid-State Circuits*, 2017, **52**(1): 151-160.

[6] Rochas A. Single photon avalanche diodes in CMOS technology [D]. Lausanne, EPFL, 2003.

[7] Niclass C, Gersbach M, Henderson R, *et al*. A single photon avalanche diode implemented in 130-nm CMOS technology [J]. *IEEE Journal of Selected Topics in Quantum Electronics*, 2007, **13**(4): 863-869.

[8] Faramarzpour N, Deen M J, Shirani S, *et al*. Fully integrated single photon avalanche diode detector in standard CMOS 0.18-μm technology [J]. *IEEE Transactions on Electron Devices*, 2008, **55**(3): 760-767.

[9] Malass I, Uhring W, Normand J P L, *et al*. A single photon avalanche detector in a 180 nm standard CMOS technology [C]. In 2015 IEEE 13th International New Circuits and Systems Conference (NEWCAS), 2015: 1-4.

[10] YANG Jia, JIN Xiang-Liang, YANG Hong-Jiao, *et al*. Design and analysis of a novel low dark count rate SPAD [J]. *J. Infrared Millim. Waves*, (**杨佳, 金湘亮, 杨红姣, 等. 一种新型低暗计数率单光子雪崩二极管的设计与分析. 红外与毫米波学报**) 2016, **35**(4): 394-397.

[11] Habib M H U, Mcfarlane N. A tunable dynamic range digital single photon avalanche diode [J]. *IEEE Electron Device Letters*, 2017, **38**(1): 60-63.

[12] Yang H, Yue X, Ping X. A high-fill-factor SPAD array cell with a shared deep N-well [C]. In 2016 China Semiconductor Technology International Conference (CSTIC), 2016: 1-3.

[13] Karami M A, Gersbach M, Yoon H J, *et al*. A new single-photon avalanche diode in 90 nm standard CMOS technology [J]. *Optics Express*, 2010, **18**(21): 22158.

[14] Finkelstein H, Hsu M J, Esener S C. STI-bounded single-photon avalanche diode in a deep-submicrometer CMOS technology [J]. *IEEE Electron Device Letters*, 2006, **27**(11): 887-889.

[15] Gersbach M, Niclass C, Charbon E, *et al*. A single photon detector implemented in a 130 nm CMOS imaging process [C]. In ESSDERC 2008 -38th European Solid-State Device Research Conference, 2008: 270-273.

[16] Richardson J A, Grant L A, Henderson R K. Low dark count single-photon avalanche diode structure compatible with standard nanometer scale CMOS technology [J]. *IEEE Photonics Technology Letters*, 2009, **21**(14): 1020-1022.

[17] Richardson J A, Grant L A, Webster E A G, *et al*. A 2 μm diameter, 9 Hz dark count, single photon avalanche diode in 130 nm CMOS technology [C]. In 2010 Proceeding of the European Solid State Device Research Conference, 2010: 257-260.

(上接第526页)

[2] Burschka J, Kessler F, Nazeeruddin M, *et al*. Co(III) complexes as p-dopants in solid-state dye-sensitized solar cells, *Chem. Mater.*, 2013, **25**: 2986-2990.

[3] Ponseca C, Savenije T, Abdellah M, *et al*. Organometal halide perovskite solar cell materials rationalized: ultrafast charge generation, high and microsecond-long balanced mobilities, and slow recombination, *J. Am. Chem. Soc.*, 2014, **136**: 5189-5192.

[4] Wehrenfenning C, Liu M, Snaith H, *et al*. Charge-carrier dynamics in vapour-deposited films of the organolead halide perovskite $CH_3NH_3PbI_{3-x}Cl_x$, *Energy. Environ. Sci.*, 2014, **7**: 2269-2275.

[5] Wehrenfenning C, Eperon G, Johnston M, *et al*. High charge carrier mobilities and lifetimes in organolead trihalide perovskites, *Adv. Mater.*, 2014, **26**: 1584-1589.

[6] Stranks S, Eperon G, Grancini G, *et al*. Electron-hole diffusion lengths exceeding 1 micrometer in an organometal trihalide perovskite absorber, *Science*, 2013, **342**: 341-344.

[7] Yamada Y, Nakamura T, Endo M, *et al*. Photocarrier recombination dynamics in perovskite CH3NH3PbI3 for solar cell applications, *J. Am. Chem. Soc.*, 2014, **136**: 11610-11613.

[8] Deschler F, Price M, Pathak S, *et al*. ? High photoluminescence efficiency and optically pumped lasing in solution-processed mixed halide perovskite semiconductors, *J. Phys. Chem. Lett.*, 2014, **5**: 1421-1426.

[9] Xing G, Mathews N, Sun S, *et al*. Long-range balanced electron-and hole-transport lengths in organic-inorganic CH3NH3PbI3, *Science*, 2013, **342**: 344-347.

[10] Marchioro A, Teuscher J, Friedrich D, *et al*. Unravelling the mechanism of photoinduced charge transfer processes in lead iodide perovskite solar cells, *Nat. Photonics*, 2014, **8**: 250-255.

[11] Manser J, Kamat P, Band filling with free charge carriers in organometal halide perovskites, *Nat. Photonics*, 2014, **8**: 737-743.

[12] Wu X, Trinh M, Niesner D, *et al*. Trap states in lead iodide perovskites, *J. Am. Chem. Soc.*, 2015, **137**: 2089-2096.

[13] Yang Y, Yang M, Li Z, *et al*. Comparison of recombination dynamics in $CH_3NH_3PbBr_3$ and CH3NH3PbI3 perovskite films: influence of exciton binding energy, *J. Phys. Chem. Lett.*, 2015, **6**: 4688-4692.

[14] Zhang B, Lv L, He T, *et al*. Active terahertz device based on optically controlled organometal halide perovskite, *Appl. Phys. Lett.*, 2015, **107**: 093301.

[15] Yoo H, Kang C, Yoon Y, *et al*. Organic conjugated material-based broadband terahertz wave modulators, *Appl. Phys. Lett.*, 2011, **99**: 061108.

[16] Yoo H, Lee S, Kang C, *et al*. Terahertz modulation on angle-dependent photoexcitation in organic-inorganic hybrid structures, *Appl. Phys. Lett.*, 2013, **103**: 151116.

[17] Matsui T, Takagi R, Takano K, *et al*. Mechanism of optical terahertz-transmission modulation in an organic/inorganic semiconductor interface and its application to active metamaterials, *Opt. Lett.*, 2013, **38**: 4632-4635.

[18] Zhang B, He T, Shen J, *et al*. Conjugated polymer-based broadband terahertz wave modulator, *Opt. Lett.*, 2014, **39**: 6110-6113.

[19] He T, Zhang B, Shen J, *et al*. High-efficiency THz modulator based on phthalocyanine-compound organic films, *Appl. Phys. Lett.*, 2015, **106**: 053303.

[20] Maeng I, Lim S, Chae S, *et al*. Gate-controlled nonlinear conductivity of Dirac fermion in graphene field-effect transistors measured by terahertz time-domain spectroscopy, *Nano Lett.*, 2012, **12**: 551.

[21] Fu M, Quan B, He J, *et al*. Ultrafast terahertz response in photoexcited, vertically grown few-layer grapheme, *Appl. Phys. Lett.*, 2016, **108**(12): 121904.

[22] Zhou Q, Shi Y, Jin B, *et al*. Ultrafast carrier dynamics and terahertz conductivity of photoexcited GaAs under electric field, *Appl. Phys. Lett.*, 2008, **93**: 102103.

[23] Yan H, An B, Fan Z, *et al*. Ultrafast terahertz probe of photoexcited free charge carriers in organometal $CH_3NH_3PbI_3$ perovskite thin film, *Appl. Phys. A*, 2016, **122**(4): 1-6.